Plectasin kills bacteria by a Ca^{2+}-sensitive supramolecular mechanism

Shehrazade Jekhmane[1,#], Maik G.N. Derks[1,2,#], Sourav Maity[3], Cornelis J. Slingerland[4], Kamaleddin H. M. E. Tehrani[4], João Medeiros-Silva[1], Vicky Charitou[1], Danique Ammerlaan[1], Céline Fetz[5], Naomi A. Consoli[6,7], Eilidh J. Matheson[8], Rachel V. K. Cochrane[8], Mick van der Weijde[1], Barend O.W. Elenbaas[1], Francesca Lavore[1], Ruud Cox[2], Joseph H.F.F Lorent[2], Marc Baldus[1], Markus Künzler[5], Moreno Lelli[6,7], Stephen Cochrane[8], Nathaniel I. Martin[4], Wouter H. Roos[3], Eefjan Breukink[2,*], Markus Weingarth[1,*]

[1]*NMR Spectroscopy, Department of Chemistry, Utrecht University, Padualaan 8, 3584 CH Utrecht, The Netherlands*

[2]*Membrane Biochemistry and Biophysics, Department of Chemistry, Utrecht University, Padualaan 8, 3584 CH, Utrecht, The Netherlands*

[3]*Moleculaire Biofysica, Zernike Instituut, Rijksuniversiteit Groningen, Nijenborgh 4, 9747 AG Groningen, The Netherlands*

[4]*Biological Chemistry Group, Institute of Biology Leiden, Leiden University, 2333 BE Leiden, The Netherlands*

[5]*Department of Biology, Institute of Microbiology, ETH Zürich, Room HCI F409, Vladimir-Prelog-Weg 4, CH-8093, Zürich, Switzerland*

[6]*Magnetic Resonance Center (CERM) and Department of Chemistry "Ugo Schiff", University of Florence, via Sacconi 6, Sesto Fiorentino, 50019 Italy*

[7]*Consorzio Interuniversitario Risonanze Magnetiche MetalloProteine (CIRMMP), via Sacconi 6, Sesto Fiorentino, 50019 Italy*

[8]*School of Chemistry and Chemical Engineering, Queen's University Belfast, David Keir Building, Stranmillis Road, Belfast, UK*

[#]equal contributions
*corresponding authors: m.h.weingarth@uu.nl, E.J.Breukink@uu.nl

Abstract
Antimicrobial resistance is a leading mortality cause, calling for the development of new antibiotics. The fungal antibiotic plectasin is the preeminent representative of eukaryotic host defense peptides that block bacterial cell wall synthesis. Here, using a combination of solid-state NMR, atomic force microscopy, and activity assays, we show that plectasin uses a new type of calcium-sensitive supramolecular killing mechanism. Efficient and selective binding of the target Lipid II, a cell wall precursor with an irreplaceable pyrophosphate, is achieved by the oligomerization of plectasin into dense supra-structures that only form on bacterial membranes that comprise Lipid II. Oligomerization and target binding of plectasin are interdependent and are enhanced by the coordination of calcium ions to plectasin's prominent anionic patch, causing allosteric changes that markedly improve the antibiotic's activity. Structural knowledge of how host defense peptides impair cell wall synthesis will enable the development of superior drug candidates.

Keywords
Antibiotics, mechanism of action, plectasin, Lipid II, solid state NMR, high speed atomic force microscopy, antimicrobial resistance, calcium

Introduction

The rise of multidrug-resistant bacteria is a severe threat to human health and calls for the development of antibiotics that use new mechanisms[1-3].

The discovery of the antibiotic plectasin, a host defense peptide isolated from the fungus *Pseudoplectania nigrella*, aroused strong interest[4,5]. Plectasin adopts a compact cysteine-stabilized fold that is representative of a large family of host defense peptides in invertebrates[4]. The peptide and its variants[6-9] show high activity against pathogens such as *methicillin-resistant Staphylococcus aureus* (MRSA), *Streptococcus pneumoniae*, or *Mycobacterium tuberculosis*, including in animal infection models[4,10]. Plectasin exerts its bactericidal activity by targeting the peptidoglycan precursor Lipid II[5] in the plasma membrane, blocking the cell wall biosynthesis.

Despite the prominence of plectasin, its mechanism is insufficiently understood. The only available molecular mechanistic data was obtained using detergent micelles[5], suggesting a conventional one-drug/one-target complex (Figure 1A). However, this binding mode appears incomplete considering recent studies that demonstrate that Lipid II-binders such as teixobactin[11,12] and clovibactin[13] use supramolecular mechanisms on the membrane surface to kill bacteria. What is more, the previously suggested complex interface[5], in which plectasin uses its β-sheet to target Lipid II, cannot fully explain functional observations. Here, the most striking observation is the small level of agreement between mutations that improve plectasin's activity[6-10] and residues that were identified in micelles[5] as relevant for Lipid II-binding. In addition, plectasin contains a conspicuous anionic patch of four consecutive negatively charged residues (9-DEDD-12) to which no function could be assigned. Together, this indicates that important aspects of plectasin's action remain elusive.

Here we report the mode of action of plectasin in biological membranes at several length scales. We show that plectasin uses a new type of supramolecular antimicrobial action that is critically enhanced by the binding of calcium ions to the anionic patch.

Results

Target binding in membranes

To study plectasin's mechanism in a relevant environment, we used solid-state NMR (ssNMR), a non-invasive technique that allows for studies of antibiotics in biological membranes at high-resolution[11]. We produced uniformly ^{13}C,^{15}N-labeled plectasin in *Escherichia coli* SHuffle® cells to ensure correct disulfide-bond topology. Solution-state NMR and activity studies confirmed the identity[4] of plectasin (Figure S1, Table 1, and Supplementary Table 1). Next, we co-assembled ^{13}C,^{15}N-plectasin and Lipid II in membranes and acquired high-quality ssNMR spectra (Figure 1B) that show the formation of a well-defined complex.

We fully assigned the chemical shifts of Lipid II-bound plectasin in membranes (Figure S2). NMR signal changes, so-called chemical shift perturbations (CSPs), between free and bound plectasin report on structural changes upon complex formation. In micelles, only minor, local signal changes in plectasin's β-sheet could be observed (Figure 1D)[5]. In contrast, in membranes, we observed marked signal changes in the entire peptide upon Lipid II-binding (Figure 1C,E). We measured not only strong signal changes in the β-sheet, which gets stabilized

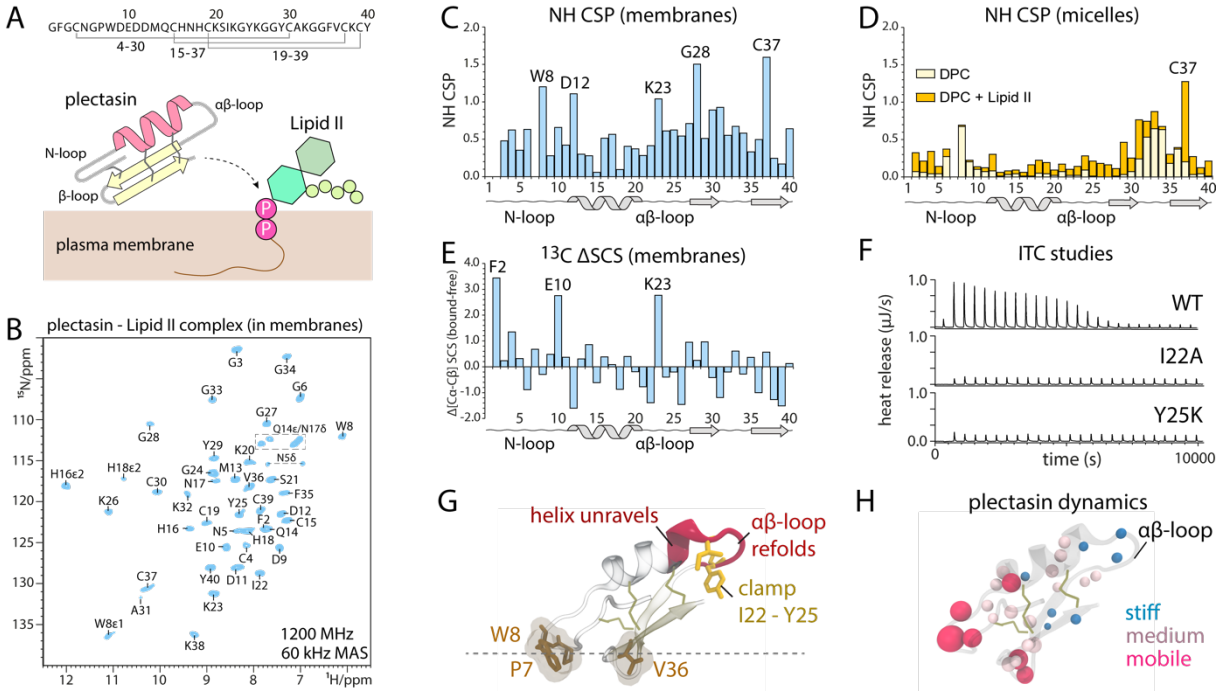

Figure 1. Plectasin's target binding in membranes. (A) Plectasin targets the peptidoglycan precursor Lipid II in the bacterial plasma membrane. The amino-acid sequence is shown, including the topology of the three disulfide bridges. (B) 2D NH ssNMR spectrum of Lipid II-bound plectasin in membranes. (C) Chemical shift perturbations (CSPs) of Lipid II-bound plectasin in membranes compared to unbound plectasin. (D) CSPs of plectasin in micelles in the presence of DPC (light yellow) and DPC plus Lipid II (dark yellow), compared to unbound plectasin. Data replotted from ref. [5]. (E) ^{13}C secondary chemical shift (SCS)[14] differences comparing unbound and Lipid II-bound plectasin in membranes (see also Supplementary Figure 2C). (F) Representative isothermal titration calorimetry (ITC) data (acquired in triplicate) show that plectasin mutants I22A and Y25K do not bind Lipid II. (G) Upon Lipid II binding, plectasin's αβ-loop changes its conformation, stabilized by a clamp-like interaction of I22 and Y25. (H) ssNMR ^{15}N T_{1rho} dynamics show that the long αβ-loop of plectasin is rigid in the Lipid II-bound state. The size of the spheres represents the dynamics per residue.

gets stabilized in the complex, but also in the αβ-loop that connects plectasin's helix and β-sheet, and in the long N-terminal loop (N-loop) around the anionic patch (D9, E10, D11, D12). As no functions were hitherto attributed to the αβ-loop or anionic patch, these observations surprised and insinuated that plectasin's action is more complex than previously reported[5]. Secondary chemical shift (SCS[14]) changes further show that the α-helix unravels at its C-terminus (S21, I22) upon Lipid II-binding, extending the αβ-loop by two residues (S21 and G27) (Figure 1E and Figure S2C).

We used mutagenesis in combination with functional studies to explore the role of the αβ-loop for plectasin's binding mechanism. Strikingly, mutants of αβ-loop residues I22 and Y25 exhibited weak or no activity toward several isolates of Gram-positive bacteria (Table 1 and Supplementary Table 1). Isothermal titration calorimetry (ITC) data show that the loss of antimicrobial activity is caused by a complete loss of binding affinity to Lipid II (Figure 1F). We surmised that the long hydrophobic and aromatic residues (I22, Y25) could be necessary to anchor plectasin to the membrane. However, ssNMR experiments that probe the interactions of plectasin with lipids or water[8] show that I22 and Y25 are not in contact with the membrane,

Table 1. Antimicrobial activity assays (under standard conditions) of plectasin mutants (minimum inhibitory concentration in μg/mL). See Supplementary Table 1 for additional activity assays.

Drug/Strain	*S. simulans 22*
Plectasin wt	0.78
I22D	>50
I22F	>50
I22K	>50
I22L	1.56
I22V	1.56
K23A	6.25
Y25F	1.56
Y25H	≤0.78
Y25I	6.25
Y25L	3.13
Y25V	6.25
K26A	3.13
K26R	≤0.78
Y29A	12.5
Y29F	1.56
Y29R	1.56
Y40R	>50
Y40F	1.56
Vancomycin	0.78

ruling out that the αβ-loop acts as a membrane anchor (Figure S3). Rather, our data show that the hinge of the N-loop (N5, P7, W8) and the β-loop/β-sheet region (Y29, A31, F35, V36) partition into the bilayer (Figure 1G). Thus, the αβ-loop may instead be involved in Lipid II binding. To test this possibility we acquired 2D CC ssNMR data and observed unambiguous contacts between the long hydrophobic sidechains of I22 and Y25 (Figure S4), suggesting that these residues form a clamp-like interaction that locks the αβ-loop in a primed conformation that is decisive for plectasin's activity (Figure 1G). This conclusion is corroborated by ssNMR relaxation data[15] that show an astonishing rigidity for the long αβ-loop in the complex, whereas the N-loop and β-loop remain highly mobile (Figure 1H and Figure S5), and it also aligns with mutagenesis data that show that hydrophobic or aromatic residues at positions 22 and 25 are required for activity (Table 1 and Supplementary Table 1).

The complex interface

Plectasin targets the cell wall precursor Lipid II, a complex C55-polyisoprenoid-based lipid with a conserved pyrophosphate (PPi) group, a headgroup composed of the sugars MurNAc and GlcNAc, and a pentapeptide (Figure 2A).

First, we investigated how plectasin targets the Lipid II-PPi group in membranes. We acquired 1D ^{31}P ssNMR spectra that show strong shifts of the PPi signals upon addition of plectasin, suggesting a direct coordination (Figure 2B). After addition of 1 equivalent of plectasin the unbound PPi peaks disappeared, indicative of the formation of an equimolar plectasin-Lipid II complex (Figure S6). Using ^{13}C-^{31}P REDOR[16] ssNMR experiments that

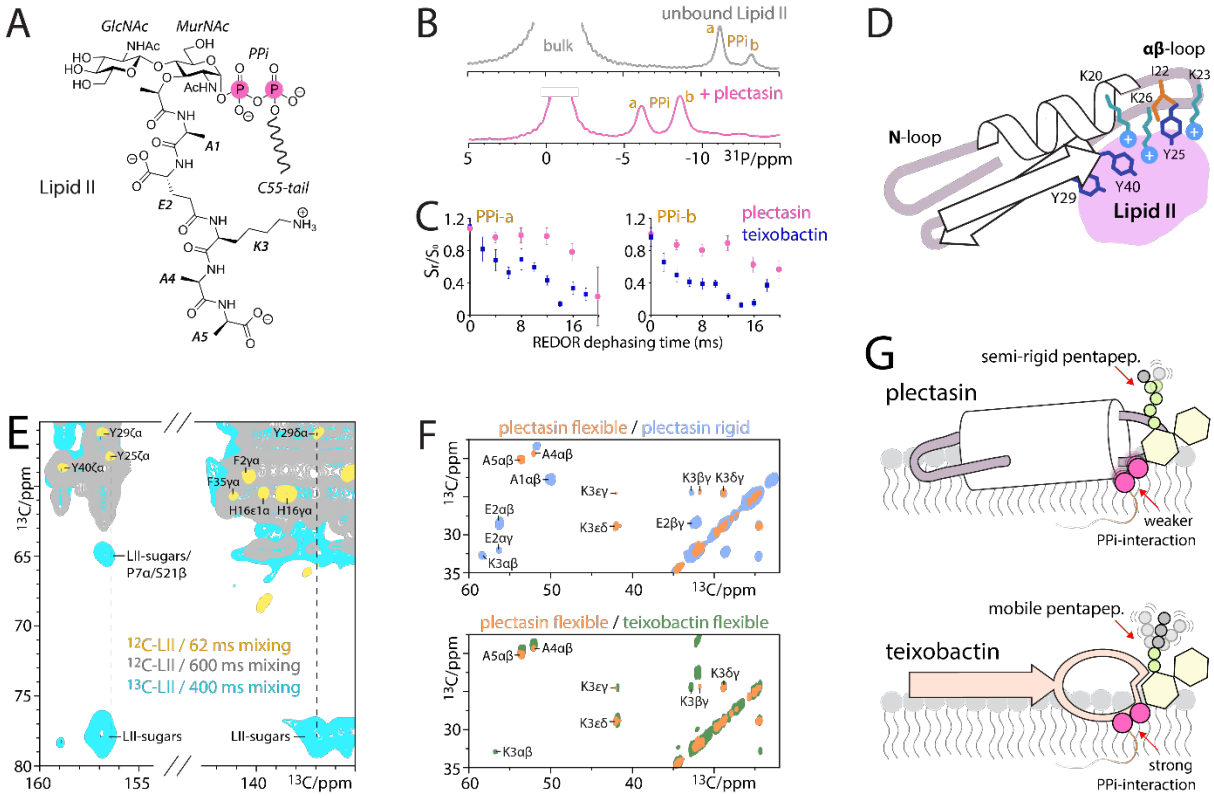

Figure 2. Lipid II binding interface. (A) Chemical structure of Lipid II. (B) 1D ^{31}P ssNMR data show strong shifts of the Lipid II pyrophosphate signals upon binding of plectasin. (C) ^{13}C-^{31}P ssNMR REDOR[16] data show slower decay of the pyrophosphate signals in the ^{13}C-plectasin - Lipid II complex compared to the ^{13}C-teixobactin - Lipid II complex. This implies that the interaction between PPi and plectasin is more dynamic. The error report one unit of standard deviation, calculated on the S_r/S_0 ratio on the bases of the experimental errors in the integrated spectra. (D) Cartoon representation of plectasin displaying the presumed residues that interact with Lipid II. (E) Overlay of 2D ssNMR ^{13}C^{13}C PARISxy[17] spectra of plectasin in complex with NMR-visible ^{13}C,^{15}N-labeled Lipid II (in cyan) and NMR-invisible ^{12}C,^{14}N Lipid II (in yellow and gray) with different CC mixing times that show contacts between aromatic residues (Y25, Y29, Y40) of plectasin and Lipid II sugars. (F) A combination of scalar[18] (that show only mobile residues) and dipolar (that show only rigid residues) 2D CC ssNMR spectra demonstrate that the pentapeptide is more flexible in the teixobactin – Lipid II complex than in the plectasin – Lipid II complex: (upper panel) Overlay of scalar (in orange) and dipolar (in blue) ssNMR spectra of the pentapeptide in the plectasin – Lipid II complex. (lower panel) Overlay of scalar ssNMR spectra of the pentapeptide in complex with plectasin (in orange) and teixobactin (in green). (G) Cartoon representations of the plectasin – Lipid II and teixobactin – Lipid II complexes.

measure the proximity between ^{13}C-labeled plectasin and PPi, we show that plectasin directly interacts with the PPi group (Figure S6). However, unlike we previously reported for teixobactin[11], we did not observe signals in 2D HP ssNMR data for the plectasin – Lipid II complex, suggesting that the plectasin – Lipid II interface is rather dynamic. The enhanced dynamics agrees with comparative ^{13}C-^{31}P ssNMR REDOR data that probe the strength of the interaction between the PPi group of Lipid II and either ^{13}C-plectasin or ^{13}C-teixobactin (Figure 2C). These data show that the teixobactin - PPi interaction is stronger compared to the plectasin – PPi interaction.

Structure-activity data (Figure 1C,E,F,H) demonstrate the essential role of plectasin's αβ-loop for Lipid II binding and antibacterial activity. It hence appears likely that the αβ-loop region, with its numerous free hydrogen bonding opportunities and its cationic residues (K20, K23, K26) is directly involved in the coordination of anionic Lipid II headgroup (Figure 2D). Indeed, mutagenesis studies show a 5-10x fold reduction in activity for the plectasin-mutants K23A and K26A (Table 1).

To explore how the Lipid II sugars contribute to the complex interface, we assembled a complex formed by $^{13}C,^{15}N$-plectasin and $^{13}C,^{15}N$-Lipid II[12] and acquired 2D CC ssNMR spectra. We could detect a unambiguous interfacial contact between Lipid II sugars and the Y29 aromatic sidechain of plectasin and a weaker unambiguous contact with the Y40 aromatic sidechain, as well as an ambiguous contact with the Y25 sidechain (Figure 2E). Mutagenesis studies (Table 1 and Supplementary Table 1) confirmed that residues 25, 29, and 40 are of functional importance. Note that the number of interfacial contacts is relatively small due to spectral overlap, but also due to the above-observed dynamics of the complex interface. Residues Y25, Y29, and Y40 are co-localized at the β-sheet - αβ-loop junction and hence point towards a molecular region that coordinates Lipid II (Figure 2E). To pinpoint the role of the Lipid II sugars, we also conducted analogous ssNMR experiments with Lipid II molecules that were specifically $^{13}C,^{15}N$-labeled at either the GlcNAc or the MurNAc sugar (Figure S7 and S8). Here, only the MurNAc sugar showed sizeable interfacial contacts, which demonstrates that MurNAc, covalently bound to PPi, is in direct proximity to plectasin, while GlcNAc is more distal to the complex interface. In accordance with these conclusions, plectasin can bind to the cognate cell wall precursor Lipid I (Figure S7), which lacks GlcNAc, although with reduced affinity[5], suggesting a role of GlcNAc beyond the direct interaction with plectasin.

Next, we analyzed the role of the Lipid II pentapeptide. Therefore, we co-assembled $^{13}C,^{15}N$-Lipid II with NMR-inactive ^{12}C-plectasin and acquired ssNMR spectra that exclusively reported on the pentapeptide in the complex (Figure 2F, S7B and S8). Dipolar 2D CC spectra, which show only rigid residues, suggested that the first four pentapeptide-residues are immobilized. This is a higher degree of immobilization than in the presence of teixobactin, that was shown not to interact with the pentapeptide[11,12] (Figure 2F, S7B). The pentapeptide's immobilization upon plectasin-binding was confirmed in a complementary scalar NMR spectrum[18] that solely reports on mobile residues and in which we only observed the C-terminal residues A4 and A5 and the sidechain of K3. Our data hence show that the backbone of residues A1-K3 is rigid, A4 is in the intermediate regime, and A5 is flexible (Figure 2G). Together, the global rigidity of the pentapeptide strongly suggests that it is directly involved in the plectasin – Lipid II interface, which aligns with the reduced activity of plectasin upon amidation of pentapeptide-residue E2 (ref. [19]).

Calcium ions enhance activity

Plectasin features a long N-terminal loop whose function is unknown, but mutations in the N-loop decisively modulate plectasin's activity[6-9]. The N-loop features a salient anionic patch (9-DEDD-12), of which we hypothesized that it could be a cation coordination site. First, we conducted ITC studies with plectasin in solution. Strikingly, ITC showed that plectasin binds bivalent cations Ca^{2+} and Mg^{2+} with high affinity (Kd = 159 ±69 nM and 195 ±35 nM, respectively) (Figure S9). To identify the cation binding site, we performed solution NMR

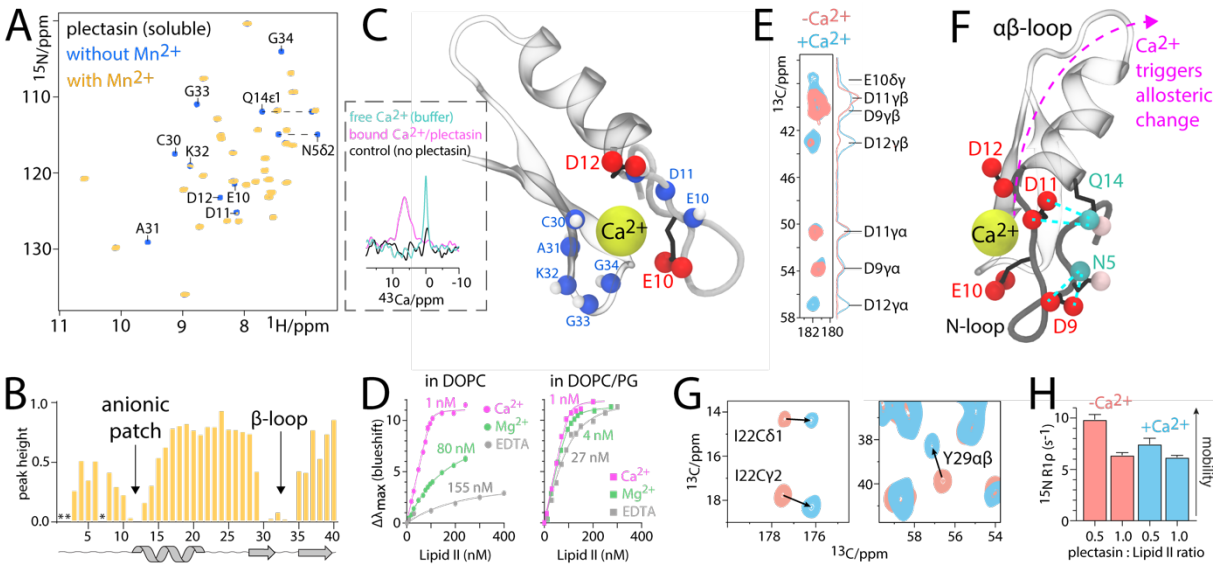

Figure 3. Ca^{2+} binds plectasin and increases Lipid II affinity. (A) 2D NH solution NMR spectra of unbound plectasin in the absence (blue) and the presence (yellow) of paramagnetic Mn^{2+}. (B) Signal intensities derived from the NMR spectrum in (A) in the presence of Mn^{2+} show that Mn^{2+} binds the anionic patch and the β-loop. Signals marked with asterisks (*) were not assigned. C) Illustration of the ion binding site. Ca^{2+} was manually modeled. The insert shows a ^{43}Ca ssNMR spectrum of Ca^{2+} (in magenta) bound to the plectasin-Lipid II complex in DOPG membranes; the control spectrum (in black) in DOPG membranes was recorded in the absence of plectasin; a spectrum of free Ca^{2+} in buffer is shown in cyan. (D) Plectasin to Lipid II binding affinities measured by tryptophan fluorescence (left panel) in zwitterionic DOPC membranes and (right panel) in anionic DOPC/DOPG membranes (1:1 mixture) with 1 mM Ca^{2+} (magenta), 1 mM Mg^{2+} (green), and in the absence of bivalent ions (100 µM EDTA, gray). (E) Dipolar ssNMR data show a rigidification of the anionic sidechains E10 and D12 of Lipid II-bound plectasin in the presence of Ca^{2+}, confirming that bivalent ions bind to the complex. (F) Sidechains D9/D11 define the conformation of the N-loop, while E10/D12 bind to Ca^{2+}. (G) Zooms into 2D PARISxy[17] CC ssNMR data show that Ca^{2+} binding allosterically modulates the αβ-loop (I22) and the β-sheet (Y29). (H) ssNMR ^{15}N T_{1rho} dynamics show that Ca^{2+} rigidifies plectasin at sub-stoichiometric plectasin to Lipid II concentrations.

Table 2. Antimicrobial activity assays of plectasin against *S. simulans* 22 at different calcium concentrations (Minimum inhibitory concentration).

Calcium (mM)	MIC (µg/mL)
0	12.5
0.31	1.56
0.5	1.56
0.63	1.56
1.25	1.56-3.13
2.5	3.13

studies with paramagnetic Mn^{2+} ions that quench the signals of plectasin residues in proximity to the ion binding site (Figure 3A,B). Upon addition of Mn^{2+}, NMR signals of the anionic patch (E10, D11, D12) and the adjacent β-loop (30-CAKGG-34) disappeared, pinpointing the ion binding pocket right below the anionic patch (Figure 3C). Finally, to directly detect Ca^{2+} binding, we acquired ^{43}Ca ssNMR spectra in liposomes (with 4 % lipid II). ^{43}Ca ssNMR in membranes showed a major shift of the ^{43}Ca signal in the presence of plectasin, conclusively demonstrating the formation of the plectasin - Ca^{2+} - lipid II complex (Figure 3C).

Next, we investigated if Ca^{2+} and Mg^{2+}, the most prominent bivalent ions in human serum, enhance the activity of plectasin. Therefore, we first investigated the binding affinity between plectasin and Lipid II using intrinsic tryptophan fluorescence, a technique that, via a blueshift of the only tryptophan-residue in plectasin (W8), reports on the peptide's membrane insertion upon Lipid II binding. Measurements were performed in neutral DOPC liposomes and in anionic DOPC/DOPG liposomes. In neutral liposomes, we observed a major Lipid II binding affinity increase by >100-fold in the presence of Ca^{2+} (Kd = 1 nM with Ca^{2+}; 155 nM without bivalent ions). This affinity increase is highly specific for Ca^{2+}, while Mg^{2+} had a much smaller effect (Kd = 80 nM). Strikingly, in anionic liposomes that mimic bacterial membranes better than neutral liposomes, the binding affinity improves (Kd = 27 nM without bivalent ions) and is less specific for the type of bivalent ion (Kd = 4 nM with Mg^{2+}), while the highest affinity is still observed in the presence of Ca^{2+} (Kd = 1 nM).

Afterwards, we conducted MIC studies in Ca^{2+}-depleted media[20] to investigate directly if the increase in binding affinity is paralleled by enhanced antimicrobial activity in the presence of Ca^{2+}. The functional assays were validated with the antibiotic daptomycin[21], whose activity strictly depends on the presence of Ca^{2+} (Figure S10). We note that Ca^{2+}-depleted media contain a high concentration (0.5 mM) of Mg^{2+}, which is essential for bacterial growth. Although to a lesser extent than in the presence of Ca^{2+}, plectasin's Lipid II affinity improves in the presence of Mg^{2+}, which suggests that the total impact of bivalent ions is underestimated in Table 2. This is presumably different for daptomycin[21], which has a very high specificity for Ca^{2+} over Mg^{2+} (ref. [21]).

To understand at the structural level how Ca^{2+}-binding affects complex formation and activity, we acquired 2D CC ssNMR spectra. After adding Ca^{2+}, the signals of plectasin's anionic E10 and D12 sidechains became more intense, implying rigidification by direct Ca^{2+}-coordination, and confirming the Ca^{2+}-binding pocket (Figure 3F). Conversely, the anionic sidechains D9 and D11 on the opposite side of the binding pocket are already rigid in the absence of calcium due to electrostatic interactions with residues N5 and Q14 that define the conformation of the N-loop (Figure 3E). Strikingly, Ca^{2+}-binding also caused long-range allosteric structural changes in the β-sheet and in the αβ-loop that are both critically involved in Lipid II binding (Figure 3G). This establishes a clear link between Ca^{2+}-coordination and target binding and offers an explanation how mutations in the N-loop, far away from the Lipid II binding site, can increase the killing activity of plectasin[6-9]. In line with this, ssNMR data show that Ca^{2+} binding changes the dynamics of the *entire* plectasin molecule (Figure 3H), causing a sizeable rigidification of the complex at a sub-stoichiometric (0.5:1) plectasin to Lipid II ratio.

Oligomerization upon target-binding

Recently, we showed that teixobactin and clovibactin form supramolecular fibrils to bind Lipid II in membranes[11,13]. Given the global effects of Ca^{2+} on plectasin's mobility and the sweeping signal differences compared to micellar data[5] (Figure 1C-E), we hypothesized that plectasin also uses a supramolecular mechanism.

To probe possible oligomerization of plectasin we used giant unilamellar vesicles (GUVs) doped with NBD-tagged Lipid II in combination with confocal microscopy. We first used a fluorescent Lipid II-variant with an NBD-fluorophore attached to lysine-3 of the

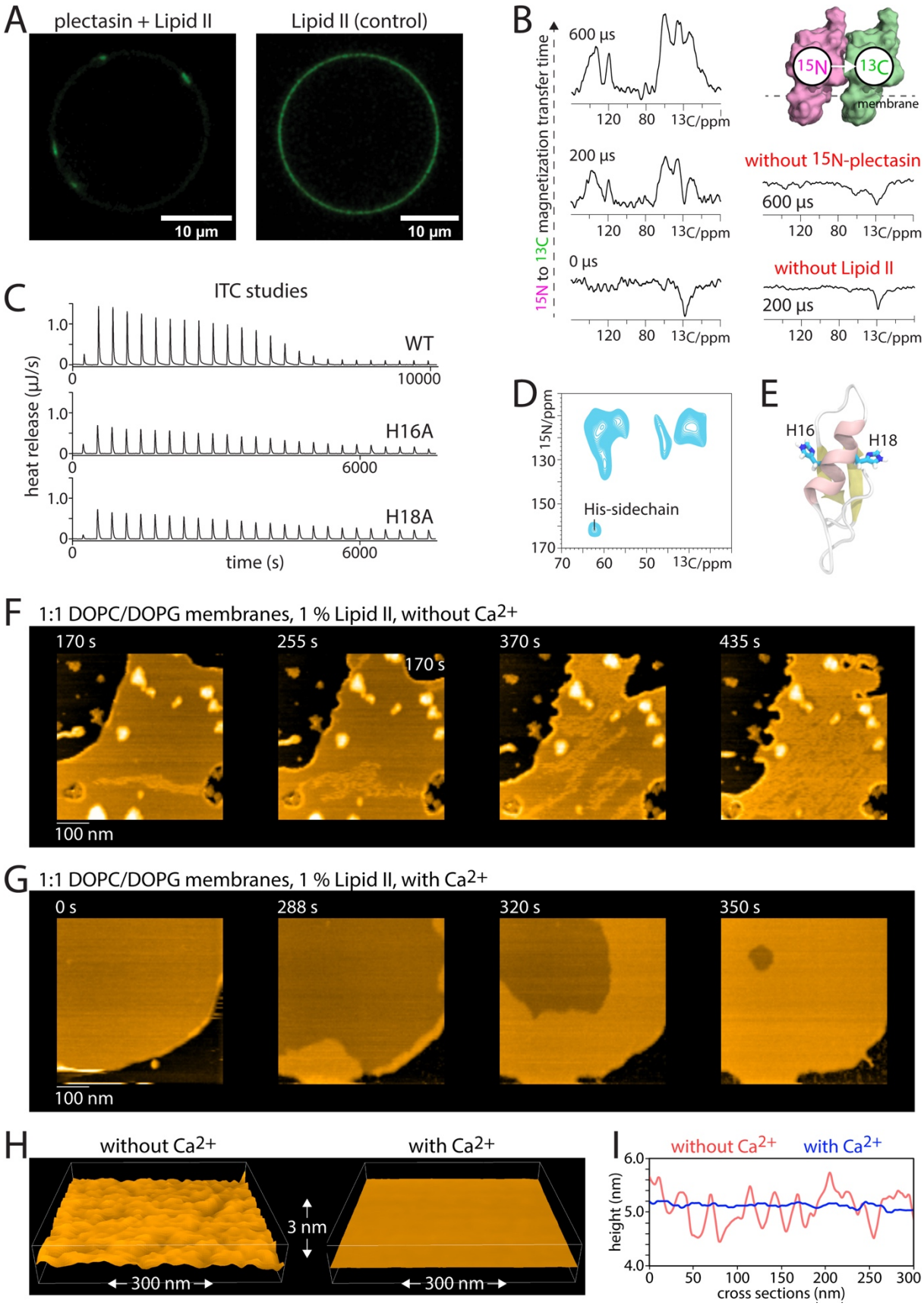

Figure 4. Plectasin oligomerizes in membranes upon Lipid II-binding. (A) Confocal microscopy of giant unilamellar vesicles (GUVs) doped with NBD-tagged Lipid II shows that plectasin induces cluster formation. (B) Plectasin oligomerization upon Lipid II-binding was probed in a FRET-like ssNMR setup[22,23] with an equimolar mixture of ^{15}N- and ^{13}C-labeled ('mixed-labeled') plectasin molecules. (left) A series of 1D DNP-

ssNMR NHHC[23] experiments with increasing ^{1}H–^{1}H magnetization transfer times applied to mixed-labeled plectasin in Lipid II-doped liposomes show the presence of plectasin oligomers. (right) Controls: The absence of signals without ^{15}N-labeling or without Lipid II show that this experiments specifically detects Lipid II-bound oligomers. (C) ITC data show that mutation of either H16 or H18 to an alanine strongly reduces Lipid II binding affinity. (D) A DNP-ssNMR 2D NHHC[23] spectrum shows the involvement of histidine sidechains in the oligomerization interface. (E) The only histidine-residues in plectasin, H16 and the conserved H18, are localized on opposite sides. (F) Snapshots of a timelapse HS-AFM video (Supplementary Video 4) following the oligomerization of plectasin in supported DOPC/DOPG lipid bilayers doped with 1 % Lipid II. (G) Same as (F) but in the presence of 1 mM Ca^{2+} (Supplementary Video 5). (H) AFM height profiles show that plectasin forms a dynamic (Supplementary Movie 6), loosely packed supra-structure (left) in the absence of Ca^{2+}, while a uniform, densely packed supra-structure is formed in the presence of Ca^{2+}. Images were taken from AFM measurements (F) and (G) after full coverage of the membranes by the plectasin supra-structures (see also Supplementary movie 7). (I) Cross-sections from the experiments shown in F) and G) illustrate the markedly different behavior of the supra-structures on the membrane surface with (in blue) and without (in red) Ca^{2+}.

pentapeptide [11,12,24]. We did not observe any oligomerization with this setup, but surmised that tagging the pentapeptide, involved in the complex interface, could interfere with plectasin's native mechanism. Therefore, we attached the NBD-fluorophore at the end of the isoprenyl tail of Lipid II (Figure S11). Indeed, with this setup, we observed cluster formation on the GUV surface after the addition of plectasin (Figure 4A), suggesting a supramolecular mechanism.

We confirmed this supramolecular mechanism by ssNMR using an NHHC[23] ssNMR experiment in combination with an equimolar mixture of ^{13}C- and ^{15}N-plectasin molecules added to Lipid II-doped liposomes. Analogously to FRET, this experiment relies on intermolecular ^{15}N to ^{13}C magnetization transfer which can only occur if ^{15}N-plectasin tightly binds ^{13}C-plectasin (Figure 4B)[22]. To avoid unspecific contacts due to crowding on the membrane surface, we worked with low Lipid II concentrations (0.5 mol%). As low concentrations compromise NMR sensitivity, we compensated by dynamic nuclear polarization (DNP) enhancement[25,26], which boosted ssNMR signal sensitivity by >50-fold (Figure S12). 1D NHHC DNP-ssNMR spectra show clear ^{15}N to ^{13}C magnetization transfer, confirming that plectasin oligomerizes upon Lipid II binding, while control experiments showed no signals (Figure 4B).

Next, we acquired a 2D NHHC DNP-ssNMR spectrum that shows that a histidine sidechain is present at the plectasin – plectasin oligomerization interface (Figure 4D and S12). This is an important observation: plectasin is flanked by two histidine residues, H16 and the highly conserved H18 (ref. [4]), that point in opposite directions (Figure 4E). Substitution of either histidine by an alanine inactivates plectasin (Supplementary Table 1), suggesting crucial binding events on both flanks. This was confirmed by ITC that showed a >10-fold loss in Lipid II binding affinity for the H16A and the H18A mutants (Figure 4C). Given that both histidine-residues, of which at least one is involved in oligomerization, critically reduce Lipid II binding capacity, our data strongly suggest that efficient oligomerization and high Lipid II-binding affinity are interdependent, which is similar to teixobactin[11].

Of note, previously it was suggested[5] that H18 would be positively charged and thereby would form a salt bridge with the anionic γ-Glu2 of the Lipid II pentapeptide. However, neither

the protonation of H18 nor the salt-bridge were experimentally observed. Indeed, our ssNMR data show that H18 and H16 sidechains are neutral[27] in the complex in membranes, refuting the purported H18 – γ-Glu2 salt bridge (Figure S13).

Oligomerization is Ca^{2+} sensitive and correlates to the MIC

To better dissect the supramolecular mechanism, we used high-speed atomic force microscopy (HS-AFM), a dynamic technique that provides biomolecular-scale resolution in real time[28,29]; recently used to study the mechanism of teixobactin[11], clovibactin[13], and AMC-109[30]. Supported bilayers of zwitterionic DOPC lipids doped with 1% Lipid II were incubated with plectasin and imaged. Within minutes, we observed the oligomerization of plectasin, starting from the membrane edge and then growing inwards into a sheet of approximately 2 nm thickness on top of the membrane (Figure S14 and Supplementary Video 1). Oligomerization was only observed in the presence of both plectasin and Lipid II (see Figure S15 for control experiments). Next, we repeated the experiments using similar conditions (DOPC membranes with 1 % Lipid II) but with 1 mM Ca^{2+}, where we observed pore formation (Figure S14 and Supplementary Video 2).

However, pore formation is very unlikely a physiologically relevant action of plectasin, because previous assays in bacteria showed no sign of membrane permeabilization[5], something that we confirmed (Figure S16). Given that AFM studies were hitherto performed with lipids carrying phosphatidylcholine (PC) headgroups that are not native to bacteria, we next wondered if plectasin's action could be sensitive to the membrane composition. An impact of the membrane composition on oligomerization would also align with our tryptophan fluorescence assays that show a marked impact of the membrane environment on plectasin's Lipid II-binding affinity (Figure 3D), and our conclusions, based on NMR-structure-activity (SAR) studies (Figure 4B-E), that binding affinity and oligomerization capacity are interdependent.

Therefore, we next conducted HS-AFM studies in membranes containing anionic lipids (1:1 DOPC:DOPG; 1 % Lipid II) in which half of the lipids carried phosphatidylglycerol (PG) headgroups that are common to bacterial membranes (Figure 4F,G,H,I and Supplementary Video 4,5). Indeed, while plectasin also rapidly oligomerized under these conditions, membrane pores were not observed in the presence of 1 mM Ca^{2+}, demonstrating that plectasin's action is sensitive to the membrane composition. Strikingly, HS-AFM data showed that Ca^{2+} drastically changed the packing of the supra-molecular assembly, which forms a densely packed carpet on the membrane surface in the presence of Ca^{2+} while the supra-structure is dynamic and heterogeneous in the absence of Ca^{2+} (Figure 4H,I). These observations agree well with ssNMR data (Figure 3H) that showed a global rigidification of plectasin in the presence of Ca^{2+}. Note that we also confirmed plectasin's sensitivity to the membrane composition and to the Ca^{2+} concentration using carboxyfluorescein (CF) leakage assays as a complementary method (Figure S17).

Altogether, as bacterial membranes are anionic and the concentration of bivalent ions high in human blood (>0.5 mM for each Ca^{2+} and Mg^{2+}), the homogeneous supra-molecular carpet mechanism that we observe in [1:1 DOPC:DOPG; 1 % Lipid II] with 1 mM Ca^{2+} is likely representative of plectasin's physiological action.

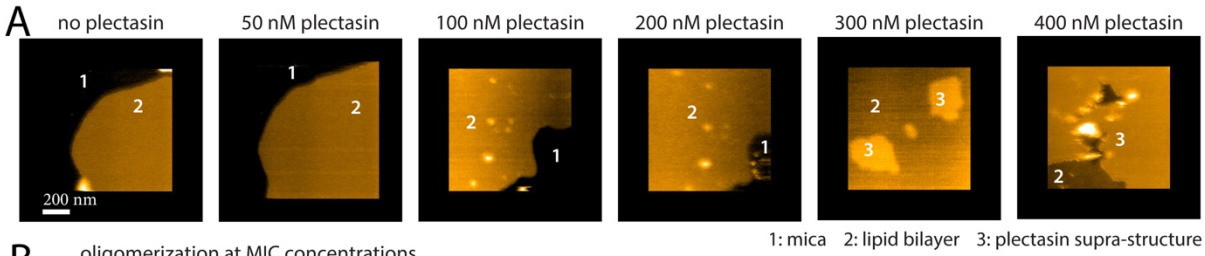
A
no plectasin
50 nM plectasin
100 nM plectasin
200 nM plectasin
300 nM plectasin
400 nM plectasin
200 nm
1: mica 2: lipid bilayer 3: plectasin supra-structure

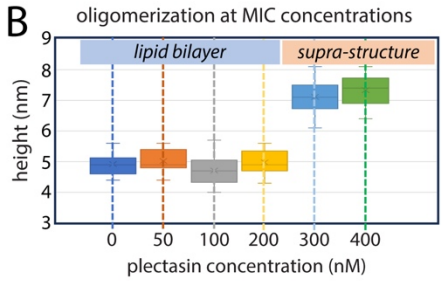
B
oligomerization at MIC concentrations
lipid bilayer
supra-structure
height (nm)
plectasin concentration (nM)

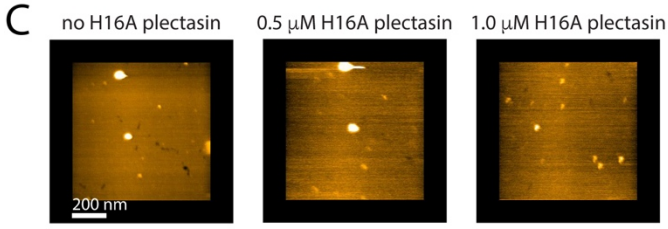
C
no H16A plectasin
0.5 μM H16A plectasin
1.0 μM H16A plectasin
200 nm

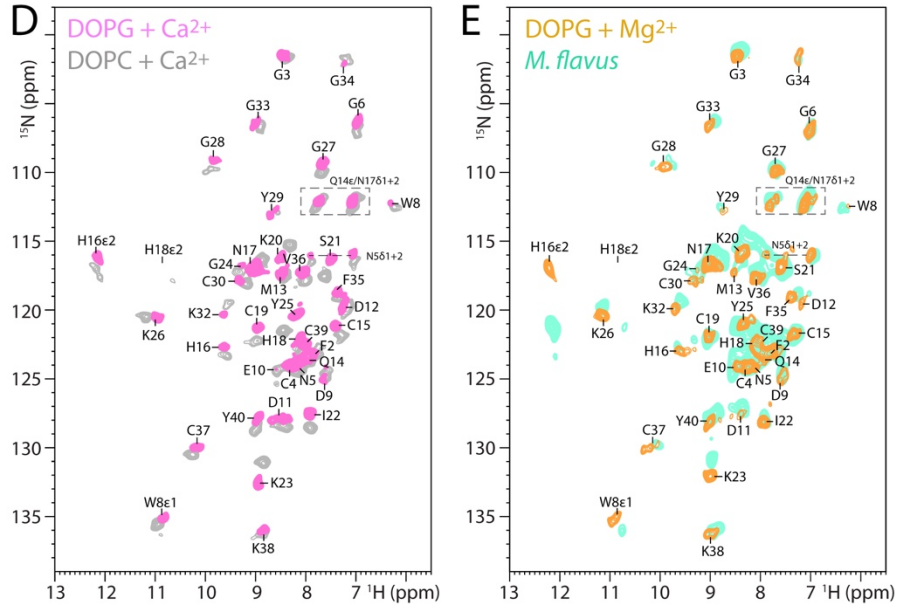
D
DOPG + Ca2+
DOPC + Ca2+
E
DOPG + Mg2+
M. flavus
15N (ppm)
1H (ppm)

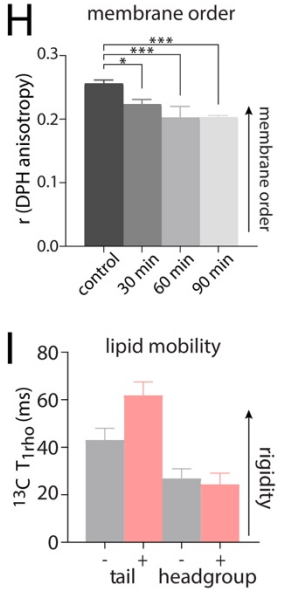
H
membrane order
r (DPH anisotropy)
control
30 min
60 min
90 min
I
lipid mobility
13C T1rho (ms)
tail
headgroup
rigidity

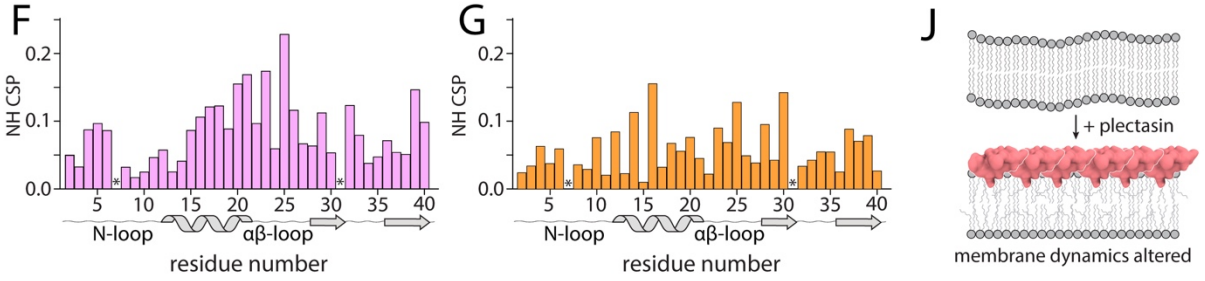
F
G
NH CSP
N-loop
αβ-loop
residue number
J
+ plectasin
membrane dynamics altered

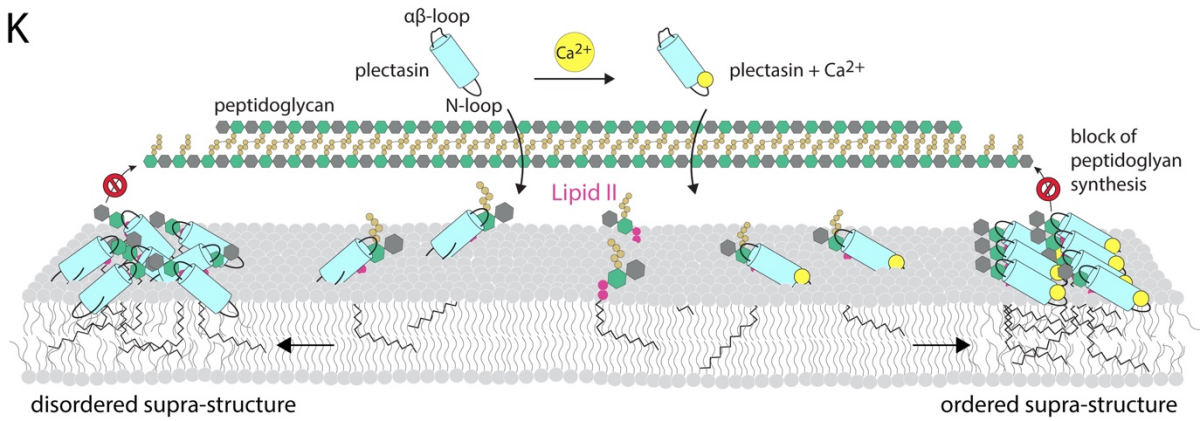
K
αβ-loop
plectasin
N-loop
Ca2+
plectasin + Ca2+
peptidoglycan
Lipid II
block of peptidoglyan synthesis
disordered supra-structure
ordered supra-structure

Figure 5. Cooperative oligomerization occurs around the MIC and affects the membrane state. (A) Plectasin AFM titration: AFM images taken before (left most image) and 10 minutes (other images) after applying plectasin at varying concentration across the MIC. Numbers indicate the regions (1) mica, (2) lipid bilayer, and (3) plectasin supra-structure layer. (B) Height distribution of membrane surface and plectasin at varying concentration show the sudden, cooperative emergence of oligomerization around MIC concentrations. The MIC of plectasin against *S. simulans* of 177 nM is indicated. (C) Snapshots of HS-AFM data taken before and 10 minutes after the addition of the H16A plectasin mutant at two different, high concentrations. No plectasin oligomerization is observed. (D) 2D NH ssNMR spectra of plectasin bound to Lipid II in the presence of Ca^{2+} in anionic DOPG (magenta) or zwitterionic DOPC (gray) liposomes. (E) 2D NH ssNMR spectra of plectasin bound to Lipid II and the presence of Mg^{2+} in DOPG liposomes (orange) and in *Micrococcus flavus* membranes (light green). Note that the H16ε2 signal is similar in both spectra but shifted due to spectral backfolding. (F) NMR signal changes (CSPs) of the two spectra shown in D). (G) CSPs of the two spectra shown in E). (H) DPH anisotropy membrane microfluidity measurements in *S. simulans* show changes in the membrane dynamics upon plectasin addition. Experiments acquired in triplicates and the error is the standard deviation. (I) ssNMR dynamics data (^{13}C-T_{1rho}) of ^{13}C-PG lipids[31] in liposomes (with 1 % Lipid II) in the presence and the absence of plectasin show that the formation of the plectasin – Lipid II complex alters the lipid mobility. The error is the standard error of the fit. (J) Scheme of the effect of plectasin binding to Lipid II on membrane dynamics. (K) Model of the Ca^{2+}-sensitive mode of action of plectasin. In the absence of Ca^{2+}, plectasin binds to Lipid II and then oligomerizes into a loosely packed supra-structure on the membrane surface. In the presence of Ca^{2+}, plectasin oligomerizes into a densely packed carpet-like supra-structure that kills bacteria more effectively.

Next, we probed if oligomerization directly contributes to plectasin's antimicrobial action. To this end, we measured AFM data as a function of the plectasin concentration using anionic DOPC/DOPG (1:1) membranes, doped with 1 % Lipid II, in the presence of 1 mM Ca^{2+} (Figure 5A,B). Strikingly, we observed a sudden emergence of supra-structures above a plectasin concentration of 200 nM (partial coverage at 300 nM of plectasin concentration, and a full coverage at 400 nM), a threshold which correlates well to the MIC of plectasin against *S. simulans* that is 0.78 μg/mL, corresponding to a plectasin concentration of 177 nM. On the other hand, oligomerization was not observed for plectasin mutant H16A, even not at a high concentration of 1 μM (Figure 5C). Together, these data strongly suggest that the formation of supra-structures is an essential part of plectasin's action. Furthermore, the sudden emergence of supra-structures above a certain threshold points to a cooperative oligomerization mechanism.

Afterwards, we investigated the impact of the membrane composition at high-resolution by ssNMR and observed signal changes in the entire plectasin molecule in anionic compared to zwitterionic lipids (Figure 5D and Figure S18), in line with a differential supramolecular packing in anionic membranes. The most pronounced signal changes were observed in plectasin's αβ-loop that is involved in Lipid II binding, linking the impact of the membrane composition on oligomerization with target binding. Next, we acquired ssNMR spectra of the plectasin – Lipid II complex directly in native cell membranes (Figure 5E and S19)[12] in the form of plasma membranes of *Micrococcus flavus* that are strongly anionic[32]. ssNMR signals in bacterial membranes overlapped closely with signals acquired in DOPG membranes in the presence of bivalent ions, demonstrating that the ssNMR data in anionic membranes with Ca^{2+}/Mg^{2+} are representative of the physiological action of plectasin. Furthermore, the high quality of the cellular ssNMR spectrum shows that the complex is well-ordered in *M. flavus*

membranes. Note that we acquired native cell membrane spectra with Mg^{2+} because Mg^{2+} is present in high concentrations during sample preparation.

We hypothesized that plectasin binding and the formation of dense antibiotic – Lipid II suprastructures interferes with the natural organization of the plasma membrane. We conducted fluorescence anisotropy assays in bacteria using DPH (1,6-diphenyl-hexa-1,3,5-triene), a compound that reports on membrane fluidity. Addition of plectasin to intact *S. simulans* cells resulted in a decrease of the fluorescence anisotropy, implying that plectasin affects the overall membrane fluidity (Figure 5H). The change in membrane fluidity was confirmed by complementary ssNMR T_{1rho} relaxation measurements of PG-lipids in liposomes (1 % Lipid II), in which we observed clear changes in the dynamics of the lipid tail and headgroup dynamics upon plectasin binding (Figure 5I). Together, our data demonstrate that plectasin's supramolecular action upon Lipid II binding affects the state of the membrane.

A widespread mechanism

Our study establishes that plectasin uses a supramolecular action. Supramolecular mechanisms are known for a few Lipid II-binding lantibiotics such as nisin[33] and were recently discovered for the depsipeptides teixobactin[11,12] and clovibactin[13]. We hence wondered if oligomerization could be a more general mechanism to sequester Lipid II. We used fluorescence microscopy to show oligomerization for different Lipid II-binders including the αβ-defensin copsin[34] and the glycopeptides teicoplanin, and ramoplanin[35] (Supplementary Figure S11). All these Lipid II-binders, of different (bacterial, fungal, and semi-synthetic) origins and chemical structures, caused the formation of Lipid II-domains in liposomes, suggesting oligomerization as a prevalent mechanism to capture cell wall precursors.

Discussion

The mechanistic data revealed in this study illuminate how plectasin targets the indispensable cell wall precursor Lipid II in membranes and paints the following picture. Settling on the membrane surface, plectasin uses long hydrophobic residues in the N-loop and αβ-loop to anchor into the membrane. Then, plectasin directly binds to conserved pyrophosphate, the MurNAc sugar, and the pentapeptide of Lipid II. ssNMR, ITC, fluorescence spectroscopy, and mutagenesis data show that the long αβ-loop of plectasin adopts a well-defined conformation that is critically required for Lipid II binding, probably by stabilizing interactions between cationic lysine sidechains and the anionic PPi or the γ-glutamate of the Lipid II pentapeptide. The specific binding of Ca^{2+} ions to the anionic patch (9-DEDD-12) in plectasin's N-loop drastically increases plectasin's binding affinity and activity. Ca^{2+} binding to monomeric plectasin rigidifies the N-loop and displaces water molecules, presumably reducing the entropic penalty for the formation of the oligomeric supra-structure. Allosterically, Ca^{2+} binding to the N-loop also changes the conformation of plectasin's β-sheet and αβ-loop, stabilizing the interaction with Lipid II. Thereby, our data establish the molecular underpinning why mutations in the N-loop, far away from the Lipid II binding site, improve plectasin's activity[6-9]. In addition, HS-AFM and ssNMR show that high-affinity binding of Ca^{2+} to plectasin fosters the formation of dense carpet-like plectasin – Lipid II supra-structures on the membrane surface. Plectasin oligomerization emerges at concentrations close to the MIC, strongly suggesting that

it is an essential part of plectasin's antimicrobial action. Oligomers emerge above a sharp concentration threshold, hinting at a cooperative event. The formation of rigid supra-structures is presumably irreversible on biological timescales, acting as a sink that concentrates Lipid II; a mesh in which Lipid II gets irretrievably entangled. These supra-structures interfere with the natural fluidity of the bacterial plasma membrane which presumably contributes to the action of plectasin[36]. Oligomerization critically requires the presence of conserved histidine residues that flank plectasin on opposition sides. Replacing the histidine-residues with alanines markedly reduces Lipid II-binding affinity, implying that Lipid II binding affinity and oligomerization capacity are interdependent, comparable to teixobactin whose activity also depends on its oligomerization capacity[11,37]. Plectasin would hence not bind to soluble PPi or PPi-containing nucleosides that are commonly present in the environment. Instead, the tight binding of plectasin to the PPi-group requires the efficient formation of a supramolecular structure on the membrane surface, significantly decreasing the k_{off} rate, i.e., increasing the residence time ($1/k_{off}$) of plectasin at its target side. Thereby, our comprehensive molecular analysis elucidates the fascinating question of how plectasin manages to tightly and selectively binds the sugar-PPi moieties of cell wall precursors (Lipid II and Lipid I) and the lack of plectasin toxicity against mammalian cells[4]. Plectasin's action against Lipid II expands our knowledge of cell wall targeting antibiotics and points the way to the design of effective new antimicrobial compounds with high selectivity. As we demonstrate with a broad array of Lipid II binding antibiotics, the formation of supra-structures emerges as a widespread mechanism to effectively and safely target cell wall precursors.

Limitations of the study

A shortcoming of our study is the limited high-resolution knowledge on the different interfaces that form the plectasin – Lipid II – Ca^{2+} suprastructure. Currently, we ignore the structural details how bivalent ions modulate the suprastructure, e.g., we do not know if bivalent ions form some kind of bridge between plectasin molecules. We are also uncertain about the finer structural details of the plectasin – plectasin interaction and the plectasin – Lipid II interaction. Furthermore, while it is clear from our data that oligomerization is an indispensable part of plectasin's action, it is uncertain if the modulation of the membrane properties by the suprastructure contributes to the antimicrobial action.

Our study also shows that plectasin can follow different oligomerization pathways, depending on the experimental conditions, i.e., depending on the membrane environment and depending on the presence or the absence of bivalent cations. We emphasize that this does not mean that plectasin would deploy different oligomerization pathways under physiological conditions, as plectasin's physiological action will always unfold in the presence of bivalent ions and in bacterial membranes that are usually anionic. However, it is a clear call to perform mode of action studies of drugs that act on membranes using experimental setups that closely resemble native conditions.

Acknowledgments

This work was funded by the Netherlands Organization for Scientific Research (NWO, grant numbers 723.014.003 & 711.018.001 to MW). This project has received funding from the European Union's Horizon Europe grant and innovation programme under grant agreement No.

101045485 (to MW). Experiments at the 950 and 1200 MHz instruments were supported by uNMR-NL, an NWO-funded Roadmap NMR Facility (no. 184.032.207). Support by Instruct-ERIC (to ML and MW) is acknowledged. Support by project INFRAIA-02-2020 PANACEA (H2020, contract no.101008500, to ML and MW) is acknowledged. ML acknowledges the Fondazione CR Firenze for funding. The present work was part of the research programme of the Netherlands Centre for One Health (www.ncoh.nl). Natural teixobactin was a kind gift from Novobiotic Pharmaceuticals.

Author contributions

MW and EB designed the study; SJ, MGND, NAC, MB, ML, and MW acquired NMR experiments; SM and WHR performed AFM experiments and data analysis; CJS, KHMET, and NIH performed activity studies; SJ, MGND, VC, and DA prepared plectasin samples; CF and MK prepared copsin samples; MGND, JMS, RC, and EB prepared Lipid II; MGND, JHFFL, MvdW, and EB ran fluorescence measurements; SJ and MGND performed ITC studies; SJ, MGND, EB, and MW prepared the manuscript and all authors edited it.

Competing interests

The authors have no competing interests.

Data availability

The NMR assignments of the plectasin – Lipid II complex in different membrane environments have been deposited in the BMRB database (accession number 51880). Experimental solid-state NMR raw data have been deposited in an open repository (DOI: 10.5281/zenodo.7985263).

Code availability

This paper does not report original code.

Methods

Plasmid construction

The coding sequence of plectasin was obtained by gene splicing by overlap extension (gene SOEing)[38] and polymerase chain reaction (PCR) gene synthesis. For the latter, Klenow fragment is used to synthesize the double-stranded DNA. Two primers were designed to amplify the plectasin gene. Afterwards, PCR was performed with the fully synthesized gene sequence for the addition of 3' adenine overhangs by Taq DNA polymerase (ThermoFisher). Plectasin was cloned into the pET SUMO TA expression vector by TA overhang cloning according to the manufacturer's specifications. Mutagenesis of plectasin was performed as described in the QuikChange II Site-Directed Mutagenesis Kit (Agilent Technologies) manual using KOD Hot Start DNA Polymerase (Novagen). Reaction mixtures were thermocycled and subsequently digested with DpnI for 1h at 37 °C. *E. coli* DH5α cells were transformed, positive colonies were selected and plasmid DNA was isolated. All plasmids were sequenced to ensure the coding sequence of plectasin mutants were correct and in-frame.

Plectasin preparation and purification

PET SUMO - plectasin was transformed into *E. coli* SHuffle® T7 cells (NEB) by heat shock according to the manufacturer's specifications. Overexpression of the 6xHis-SUMO-plectasin fusion protein was accomplished following the protocol of ref[39]. Expression of 6xHis-SUMO-plectasin was induced in 1L ^{13}C,^{15}N-labeled M9 medium at an OD_{600} of 0.6 using 0.5 mM IPTG for a period of 4 h at 37 °C. Cells were harvested by centrifugation at 4,000 × g at 4 °C for 30 min. Bacterial pellets were resuspended in lysis buffer (50 mM sodium phosphate, 150 mM NaCl, 25 mM imidazole, and 1 mM β-mercaptoethanol, pH 8.0) supplemented with 200 µg/mL chicken egg white lysozyme and 1 µg/mL DNase I. The suspension was sonicated and cellular debris was removed by centrifuging at 40,000 × g for 30 min. The supernatant was filtered through a 0.45 µm filter. The 6xHis-SUMO-plectasin fusion protein was purified by affinity chromatography using pre-equilibrated Ni-NTA resin (Qiagen). The sample was repeatedly (5x) applied to the resin and subsequently washed with 20 column volumes (CV) of wash buffer (50 mM sodium phosphate, 150 mM NaCl, 25 mM imidazole, and 1 mM β-mercaptoethanol, pH 8.0) and eluted with 2 CV of elution buffer (50 mM phosphate buffer, 150 mM NaCl, 400 mM imidazole, and 1 mM β-mercaptoethanol, pH 8.0). Afterwards, SUMO protease was added at a 1:1000 molar ratio to the purified fusion protein and incubated o/n at 4 °C. Further purification of plectasin was accomplished by Size Exclusion Chromatography on a Superdex 30 Hiload 26/60 column at a flow rate of 2.6 mL/min with 50 mM sodium phosphate, 150 mL NaCl, and 1 mM β-mercaptoethanol, pH 7.2. Fractions corresponding with pure plectasin were collected and stored at -20 °C and concentrated and/or buffer exchanged to the desired concentration using a 3.5 kDa cutoff Amicon Ultra filter unit (Millipore) before use.

Synthesis of Lipid II and cell wall precursors

Lipid II was synthesized and purified as previously described[40]. In short, Lipid II was reconstituted enzymatically from undecaprenyl phosphate, UDP-GlcNAc, and UDP-MurNAc-pentapeptide with MurG and mraY and purified on DEAE cellulose. Undecaprenyl was isolated from *Laurus nobilis* and subsequently enzymatically phosphorylated[41]. $^{13}C^{15}N$-labeled UDP-GlcNAc and UDP-MurNAc-pentapeptide were extracted from *B. cereus* and *S. simulans* respectively grown in $^{13}C^{15}N$-labeled medium consisting of M9 supplemented with $^{13}C^{15}N$-Silantes, $^{13}C^{15}N$-Bioexpress, U-^{13}C-glucose, and ^{15}N-NH_4Cl after accumulation of the precursors using fosfomycin or vancomycin and moenomycin. Undecaprenol ω-azide was synthesized as previously described[42]. Trichloroacetonitrile (784 µL, 78.0 µmol, 6.0 equiv.) was added to a solution of undecaprenol ω-azide (10.0 mg, 13.0 µmol) in anhydrous dichloromethane (1 mL), and the resulting solution stirred at ambient temperature for 1 h. A solution of tetrabutylammonium dihydrogen phosphate (17.7 mg, 52.0 µmol, 4.0 equiv.) in anhydrous dichloromethane (1 mL) was then added dropwise and the resulting solution refluxed overnight. The reaction mixture was concentrated *in vacuo*, redissolved in THF (1 mL) and 25% aqueous ammonium hydroxide (0.2 mL), and stirred for 30 min. Toluene (2.5 mL) and methanol (2.5 mL) were then added, the mixture stirred for 20 min, filtered, and concentrated *in vacuo*. The resulting oil was washed with petroleum ether (3 x 5 mL) and redissolved in methanol (2 mL). Excess ammonium form DOWEX 50WX8 resin was added, the mixture stirred for 30 min, filtered, and concentrated *in vacuo*. The resulting crude oil was purified by

flash column chromatography (SiO_2, 65:25:5 chloroform:methanol:0.1% aqueous ammonium hydroxide) to yield the product as a clear oil (5.0 mg, 44%). Und-NBD-Lipid II was synthesized by reconstitution from UndP-N_3 as described for native Lipid II, followed by addition of the tag *via* copper-catalyzed cycloaddition with alkyne-NBD. N_3-LII, $CuSO_4$, and THPTA were premixed in 10 mM Tris-HCl buffer at pH = 8.0 and stirred at RT for 20 minutes. Then, sodium ascorbate was added and the mixture dried under a flow of N_2. The residue was redissolved in H_2O and added 1:1 (v/v) to a premixed solution of Und-N_3-Lipid II and NBD-alkyne in MeOH to final concentrations of $CuSO_4$ (0.1 mM), THPTA (0.5 mM), sodium ascorbate (1 mM), Und-N_3-Lipid II (0.1 mM), and NBD-alkyne (0.3 mM). The reaction was protected from light and stirred at RT overnight and purified as described for unmodified Lipid II. Lipid concentrations were measured as inorganic phosphate after treatment with perchloric acid[43].

Isothermal titration calorimetry (ITC)

200 nm large unilamellar vesicles (LUVs) were prepared from 2 mol% Lipid II in DOPC by the extrusion technique[44]. ITC measurements were conducted on a low-volume Affinity ITC (TA instruments). All measurements were conducted at 37 °C. Samples were degassed for 10 min prior to the ITC experiments. The cell was filled with plectasin (in 50 mM HEPES, 150 mM NaCl at pH = 7.2) and titrated with LUVs in the same buffer under constant stirring at 125 rpm. The data was analyzed using the Nano Analyze software (TA Instruments). After baseline correction the integrated peaks were fitted using an independent binding model. Each measurement was acquired in duplicate.

NMR sample preparation

Solution NMR samples were prepared by adding 10% D_2O to 20-50 µM plectasin in 50 mM phosphate, 150 mM NaCl at pH = 7.2.

Unless specified otherwise, ssNMR samples contained multi-lamellar vesicles (MLVs) of DOPC doped with 4 mol% Lipid II (lysine form) at a final molar ratio of 1:1 plectasin/Lipid II in phosphate buffer (50 mM sodium phosphate, 150 mM NaCl at pH = 7.2). For experiments done in the presence of Ca^{2+} we used HEPES buffer (50 mM HEPES, 150 mM NaCl at pH = 7.2). Appropriate lipid stocks in chloroform or 2:1 chloroform/methanol were mixed in a glass tube, dried under a flow of N_2 with gentle heating and then exposed to high vacuum for 20 mins to form lipid films. Films were then hydrated by the addition of plectasin in buffer, followed by extensive vortexing. The resulting vesicles were collected by ultracentrifugation at 100,000 × g for 30 min at 4 °C. This co-assembly sample preparation strategy ensures that plectasin is present on both sides of the membranes, including in the inner vesicles of MLVs, and thus is able to reach all the Lipid II molecules in the MLVs. Subsequently, liposomes were directly centrifuged into ssNMR MAS rotors. For the $^{15}N(^1H^1H)^{13}C$ experiments we used 0.5 mol% Lipid II in DOPC and an equimolar mixture of ^{13}C-enriched plectasin ($^{14}N^{13}C$-plectasin, i.e., N at natural abundance) and ^{15}N-enriched plectasin ($^{15}N^{12}C$-plectasin, i.e., C at natural abundance) in the presence of 15 mM AMUPol[45] in 60% glycerol-d8, 35% buffer in D_2O (to same final salt concentrations described above), and 5% H_2O. Samples were loaded into sapphire 3.2 mm rotors. For ^{43}Ca ssNMR experiments, 0.5 mM $^{43}CaCO_3$ (84.8 ± 0.8% isotopic enrichment) was added to plectasin in buffer prior to hydration of 4 mol% Lipid II in DOPG lipid films. As a

control, we made an identical sample only omitting plectasin in the buffer. After sample collection by centrifugation only plectasin-bound calcium is concentrated in the pellet. Additionally, one sample was made containing only 10 mM ^{43}Ca in buffer as a control for unbound Ca^{2+}.

Bacterial membrane vesicles with reconstituted Lipid II were prepared essentially as previously described[32]. In short: Micrococcus flavus DSM 1790 or Staphylococcus simulans 22 were grown to late log phase in TSB, harvested by centrifugation, washed once with buffer (50 mM phosphate, 50 mM NaCl pH 8.0), and lysed using a cell disruptor (Constant Systems) in the presence of lysozyme, benzonase, and 1 mM $MgSO_4$. Debris was removed by low-speed centrifugation (4,000 × g, 4 °C, 15 min) and large membrane vesicles were collected by high-speed centrifugation (40,000 × g, 4 °C, 1 h). Lipid II was reconstituted in the presence of 3 mM $MgSO_4$ and an excess of Lipid II precursors UDP-MurNAc-pentapeptide and UDP-GlcNAc. Reagents were mixed with 4 freeze-thaw cycles on ice, followed by a 30 min incubation at RT. ^{15}N-plectasin was then added and after 2 more freeze-thaw cycles the vesicles were collected by ultracentrifugation (175,000 × g, 4 °C, 90 min) and spun down into 1.3 mm rotors.

Solid state NMR experiments

^{1}H-detected experiments were carried out at 60 kHz MAS and magnetic fields of 16.4, 18.8 T, and 28.2 T (700, 800, and 1200 MHz ^{1}H frequency) and a sample temperature of approximately 305 K. PISSARRO low-power proton decoupling was applied in all dimensions[46,47]. ^{13}C-detected experiments were carried out at 16.4, 18.8 or 22.3 T (700, 800, or 950 MHz ^{1}H frequency). Dipolar-based 2D ^{13}C-^{13}C spectra were recorded at a sample temperature of 270 K using PARISxy[17,48] recoupling (m = 1 at 16.4 T and m = 2, 10 kHz recoupling amplitude, 20 – 1000 ms mixing time) and SPINAL64 decoupling[49]. Chemical shift assignments were obtained using ^{1}H-detected 3D CαNH, Cα(CO)NH, and CO(Cα)NH experiments as previously described[50], combined with 2D ^{13}C-^{13}C PARISxy[17,48] experiments with different mixing times. A 2D scalar $^{13}C^{13}C$ TOBSY[18] experiment was conducted with 8 kHz MAS at 295 K sample temperature with 6 ms ^{13}C-^{13}C mixing time. Mobility edited 2D $^{1}H(^{1}H)^{13}C$ experiments[51] were performed at 700 MHz, 16.5 kHz MAS, and a sample temperature of 300 K. A ^{1}H T_2 relaxation filter of 3.5 ms was used. Magnetization from mobile lipids and water was transferred to the rigid antibiotic with a ^{1}H-^{1}H mixing time of 7 ms, followed by a short cross-polarization step (175 µs) to ^{13}C nuclei. DNP-enhanced $^{15}N(^{1}H^{1}H)^{13}C$ experiments[23] were carried out at 9.4 T (400 MHz ^{1}H frequency) at 8 kHz MAS and at 100 K. Very short contact times (80 µs) for the second and third CP steps were used and the ^{1}H-^{1}H mixing time was set to 200 µs. 1D ^{43}Ca ssNMR spectra were recorded in 2.5 mm rotors, at 18.8 T (800 MHz ^{1}H frequency), 10/15 kHz MAS, and a sample temperature of 285 K using direct polarization and no decoupling. ^{31}P ssNMR spectra were recorded at 11.7 for 1D cp spectra or 18.8 T for REDOR experiments (500 and 800 MHz ^{1}H frequency respectively). 1D CP ^{31}P spectra were recorded with 13.5 kHz MAS and a sample temperature of 280 K. $^{31}P\{^{13}C\}$c-REDOR[52] experiments were conducted at 60 kHz MAS and a sample temperature of 290 K using 15 kHz SW_f-TPPM[53] ^{1}H decoupling during dephasing and acquisition. Dephased (S_r) and reference (S_0) spectra were recorded using 0, 4, 8, 12, 16, and 20 ms dephasing times. The analysis of the REDOR data is described in the

Supplementary Information. ^{1}H-detected ^{15}N T_{1rho} relaxation experiments[15] were used to measure the dynamics of Lipid II-bound plectasin in membranes at fast (60 kHz) MAS. ^{1}H-detected ^{13}C T_1 and T_{1rho} experiments were used to measure the dynamics of ^{13}C-labeled PG lipids[31] in liposomes (89 mol% DOPG, 10 mol% ^{13}C-labeled PG isolated from *S. simulans*, 1 mol% Lipid II) with and without plectasin. Spectra were recorded at 16.4 T (700 MHz ^{1}H frequency), 58 kHz MAS, and a sample temperature of approximately 305 K. Relaxation data were fitted in Prism and the error shows the standard error of the fit.

Solution state NMR experiments

Backbone assignments of plectasin were obtained using 3D CαNH, CαCβNH, CONH, and CβCα(CO)NH experiments at magnetic fields of 21.1 or 14.1 T (900 or 600 MHz ^{1}H frequency). Backbone amide dynamics were determined at 14.1 T (600 MHz ^{1}H frequency) at 298 K. ^{15}N-T_1 relaxation times were determined using relaxation delays of 0.01, 0.05 (x2), 0.10, 0.20, 0.40 (x2), 0.7, 1 and 1.4 s. ^{15}N-T_2 relaxation times were extracted from ^{15}N-$T_{1\rho}$ measurements as previously described[54]. ^{15}N-$T_{1\rho}$ relaxation times were determined using a spin-lock pulse of 1.9 kHz of 4, 16 (x2), 32, 48, 80, 112 (x2), 128, 160, 208, and 256 ms. Trajectories were fit to single exponentials.

Microscopy

GUVs were prepared by electroformation using in-house build Teflon cells with two titanium wires as electrodes. 1 µL of 0.5 mM DOPC with 0.4 mol% NBD-Lipid II in 2:1 CHCl3/MeOH was brushed on both electrodes and thoroughly dried under vacuum. Next, the cell was filled with 350 µL 300 mM sucrose and GUVs were formed by applying an oscillating voltage (sine wave, 2 V, 10 Hz) for 90 minutes and released from the electrodes (square wave, 2 V, 2 Hz). Microscopy slides were precoated using a 1 mg/mL BSA solution. Slides were filled with 300 µL 300 mM glucose solution, followed by addition of the antibiotic and finally 30-50 µL GUV solution. The GUVs were imaged using a Zeiss LSM 880 confocal microscope with an x63/1.2NA glycerol objective lens. Green fluorescence (530-545 nm) was detected after excitation with a 488 nm laser.

Carboxyfluorescein leakage

Vesicle leakage assays were conducted using LUVs filled with carboxyfluorescein (CF). CF solutions were made by suspending ~50 mM CF in H_2O and adjusting the pH to ~7.2 using 10 M NaOH. The resulting solution was diluted with H_2O to match the osmolarity of the outside buffer (OB), which consisted of 10 mM Tris, 100 mM NaCl, pH=7.2. LUVs were prepared as described above. Non-enclosed CF was removed using a Sephadex G50 column equilibrated in OB. Measurements were conducted on a Cary Eclipse spectrophotometer at 20 °C under constant stirring by monitoring the fluorescence intensity at 515 nm (excitation at 492 nm, 5 nm slit width, 0.1 s averaging time). A total lipid concentration of 25 µM was used for all experiments. Fluorescence traces were normalized using the fluorescence baseline at the start as 0% and fluorescence after treatment with 0.1 vol% Triton-X100 as 100%.

Tryptophan fluorescence spectroscopy

Plectasin's single tryptophan can be used to monitor insertion into the membrane. Measurements were done on a Cary Eclipse (FL0904M005) fluorimeter at 20 °C under constant stirring in a 4x10 mm quartz cuvette. For titration experiments the cuvette was oriented perpendicular to the excitation beam to minimize scattering. LUVs with or without 2 mol% Lipid II (prepared as described above at 1-5 mM total lipid concentration) were titrated to 100 nM plectasin in 50 mM HEPES, 150 mM NaCl at pH = 7.2. Fluorescence was excited at 280 nm (5 nm slit) and recorded between 300 and 400 nm (10 nm slit) at 1 nm intervals with 1 second averaging per point. Spectra were corrected for a blank using buffer and for scattering using a titration series in the absence of plectasin. Corrected spectra were fit with log-normal distributions and the shift of resulting wavelength of maximum fluorescence ($\Delta\lambda_{max}$) as a function of Lipid II concentration on the outside of the vesicles were fit using a quadratic binding equation[55] to obtain the binding affinities.

Bacterial permeabilization assay

Overnight cultures (37 °C, TSB) of *S. simulans* were diluted to OD_{600} = 0.1 and grown until mid-log phase (OD_{600} = 0.5-0.8) and harvested by centrifugation (2,000 × g, RT, 5 min). Cell pellets were washed with buffer (10 mM Tris, 50 mM NaCl and 0.5 w/v% glucose at pH = 7.2) and resuspended to OD_{600} = 10 and stored at 4 °C until use. All assays were performed on a Cary Eclipse (FL0904M005) fluorometer. Measurements were done using bacterial suspensions at OD_{600} = 0.05 in the aforementioned buffer under constant stirring at 20 °C in a 4x10 mm quartz cuvette. 0.2 µM $DiSC_2(5)$ or 0.25 µM SYTOX green was added and equilibrated for 2 minutes before addition of an antibiotic. For $DiSC_2(5)$ we used excitation and emission wavelengths of 650 nm and 670 nm respectively, while for SYTOX green we used 504 nm and 523 nm. 5 nm slits were used, and fluorescence signal was averaged every 0.3 seconds.

DPH anisotropy measurements

Preparation of *S. simulans* stock solutions was done as described above for bacterial permeabilization in PBS. 1 mL of a cell suspension of OD_{600} = 0.1 in PBS was treated with 1 µM plectasin and incubated at 37 °C. All assays were performed on a Cary Eclipse (FL0904M005) fluorometer fitted with a manual polarizer accessory (Varian). Measurements were conducted at 37 °C under constant stirring in a 4x10 mm quartz cuvette. 10 µM DPH was added from a 1 mM stock in DMSO (bringing the final DMSO concentration to 1 v%) and incubated for 5 minutes. Fluorescence was excited with 380 nm light (10 nm slit) and recorded between 430 and 520 nm (10 nm slit) with 0.5 s averaging time and data interval of 1.66 nm per point. Fluorescence anisotropy was calculated using the maximum intensity of each spectrum according to the equation:

$$r = \frac{I_{VV} - I_{VH}}{I_{VV} + 2I_{VH}}$$

MIC assays under standard conditions

Plectasin and analogues were serially diluted in cation-adjusted Mueller-Hinton broth (CAMHB) in round-bottom polypropylene 96-well plates (50 µL/well). Selected bacterial strains were grown from glycerol stocks on blood agar plates. Individual colonies were inoculated in tryptic soy broth (TSB) and incubated at 37 °C while shaking until OD_{600} reached 0.5. Bacterial suspensions were then diluted 100 times in CAMHB and distributed (50 µL/well) over the microplate containing the diluted plectasin solutions. Plates were covered by a gas-permeable adhesive membrane, and incubated at 37 °C while shaking. Minimum inhibitory concentrations (MICs) were determined by visual inspection after 16-20 hours (*Staphylococcus*) or 20-24 hours (*Streptococcus*). For *Streptococcus* strains, the broth was additionally supplemented with 5% lysed horse blood and the microplates were incubated under 5% CO_2 atmosphere. In the assays, we used the following strains: *Staphylococcus simulans*, *Streptococcus pneumoniae serotype 8*, *S. pneumoniae ATCC6305*, and *Streptococcus pyogenes* M3.

Ca^{2+} variable MIC assays

Cation-depleted MHB was prepared as previously described[20] and supplemented with $MgCl_2$ (0.5 mM) and $ZnSO_4$ (10 µM). Plectasin was serially diluted 2-fold over a 96-well polypropylene plate. Serial dilutions of Ca^{2+} in calcium-depleted medium were subsequently added to the wells containing the plectasin dilution series, followed by addition of bacterial suspensions. Minimum inhibitory concentrations (MICs) were determined by visual inspection after 16-20 hours (*Staphylococcus*). The effect of reduced Ca^{2+} levels on *S. simulans* growth in the absence of plectasin was assessed by monitoring growth at 37°C by OD_{600} over 18 hours (see Figure S20).

High-speed AFM

HS-AFM imaging was performed on a supported lipid bilayer deposited on mica using an amplitude modulation tapping mode HS-AFM from RIBM, Japan (Ando type)[11]. The lipid compositions are as stated in the experimental conditions of the corresponding results. Short cantilevers (~7 µm) with a nominal spring constant of 0.15 N/m were used (USC-F1.2-k0.15, NanoWorld, Switzerland) for all experiments. A minimal imaging force was applied by using a small set-point amplitude, typically 80% of the free amplitude (for 1-2 nm of free amplitude). The lipid bilayer was obtained by incubating LUVs (at a total lipid concentration of 0.5 mg/ml) containing synthetic lipids (as stated in the manuscript) with or without Lipid II (prepared as mentioned above) on top of freshly cleaved mica for 30-40 minutes. After the incubation period, the mica was cleaned gently using recording buffer (10 mM Tris-Cl, 100 mM NaCl, pH 7.2 with or without 1 mM $CaCl_2$). Imaging was started on the lipid bilayer surface in recording buffer. Next, a concentrated plectasin solution was added to reach the desired final concentration of plectasin in the 40 µl AFM chamber. The results reported at varying plectasin concentrations (Figure 5 A), or varying H16A plectasin mutant concentrations (Figure 5 C) were performed on the same sample by adding additional plectasin (or the mutant) on the AFM sample chamber to reach the corresponding final concentration. Image analysis was done using Igor Pro (Wavemetrics, Lake Oswego, OR, USA) and ImageJ with minimal image corrections (tilt, drift, and background corrections). The time stamps on HS-AFM movies are relative to

plectasin addition into the liquid chamber. Image acquisition rate varied from 0.5 frames/second to 2 frames/second (see figure/movie legend).

References

1 Lewis, K. The Science of Antibiotic Discovery. *Cell* **181**, 29-45, doi:10.1016/j.cell.2020.02.056 (2020).

2 Brown, E. D. & Wright, G. D. Antibacterial drug discovery in the resistance era. *Nature* **529**, 336-343, doi:10.1038/nature17042 (2016).

3 Cook, M. A. & Wright, G. D. The past, present, and future of antibiotics. *Science Translational Medicine* **14**, doi:10.1126/scitranslmed.abo7793 (2022).

4 Mygind, P. H. *et al.* Plectasin is a peptide antibiotic with therapeutic potential from a saprophytic fungus. *Nature* **437**, 975-980, doi:10.1038/nature04051 (2005).

5 Schneider, T. *et al.* Plectasin, a Fungal Defensin, Targets the Bacterial Cell Wall Precursor Lipid II. *Science* **328**, 1168-1172, doi:10.1126/science.1185723 (2010).

6 Ostergaard, C., Sandvang, D., Frimodt-Moller, N. & Kristensen, H. H. High cerebrospinal fluid (CSF) penetration and potent bactericidal activity in CSF of NZ2114, a novel plectasin variant, during experimental pneumococcal meningitis. *Antimicrob Agents Chemother* **53**, 1581-1585, doi:10.1128/AAC.01202-08 (2009).

7 Brinch, K. S. *et al.* Intracellular activity of the peptide antibiotic NZ2114: studies with Staphylococcus aureus and human THP-1 monocytes, and comparison with daptomycin and vancomycin. *J Antimicrob Chemother* **65**, 1720-1724, doi:10.1093/jac/dkq159 (2010).

8 Zhang, Y. *et al.* In vitro and in vivo characterization of a new recombinant antimicrobial peptide, MP1102, against methicillin-resistant Staphylococcus aureus. *Appl Microbiol Biotechnol* **99**, 6255-6266, doi:10.1007/s00253-015-6394-7 (2015).

9 Tenland, E. *et al.* A novel derivative of the fungal antimicrobial peptide plectasin is active against Mycobacterium tuberculosis. *Tuberculosis (Edinb)* **113**, 231-238, doi:10.1016/j.tube.2018.10.008 (2018).

10 Brinch, K. S. *et al.* Plectasin Shows Intracellular Activity against Staphylococcus aureus in Human THP-1 Monocytes and in a Mouse Peritonitis Model. *Antimicrobial Agents and Chemotherapy* **53**, 4801-4808, doi:10.1128/aac.00685-09 (2009).

11 Shukla, R. *et al.* Teixobactin kills bacteria by a two-pronged attack on the cell envelope. *Nature* **608**, 390-396, doi:10.1038/s41586-022-05019-y (2022).

12 Shukla, R. *et al.* Mode of action of teixobactins in cellular membranes. *Nature Communications* **11**, doi:10.1038/s41467-020-16600-2 (2020).

13 Shukla, R. *et al.* An antibiotic from an uncultured bacterium binds to an immutable target. *Cell* **186**, 4059-4073.e4027, doi:10.1016/j.cell.2023.07.038 (2023).

14 Wang, Y. Probability-based protein secondary structure identification using combined NMR chemical-shift data. *Protein Science* **11**, 852-861, doi:10.1110/ps.3180102 (2002).

15 Jekhmane, S. *et al.* Shifts in the selectivity filter dynamics cause modal gating in K+ channels. *Nature Communications* **10**, doi:10.1038/s41467-018-07973-6 (2019).

16 Gullion, T. & Schaefer, J. Rotational-echo double-resonance NMR. *Journal of Magnetic Resonance (1969)* **81**, 196-200, doi:10.1016/0022-2364(89)90280-1 (1989).

17 Weingarth, M., Bodenhausen, G. & Tekely, P. Broadband magnetization transfer using moderate radio-frequency fields for NMR with very high static fields and spinning speeds. *Chemical Physics Letters* **488**, 10-16, doi:10.1016/j.cplett.2010.01.072 (2010).

18 Baldus, M. & Meier, B. H. Total Correlation Spectroscopy in the Solid State. The Use of Scalar Couplings to Determine the Through-Bond Connectivity. *Journal of Magnetic Resonance, Series A* **121**, 65-69, doi:10.1006/jmra.1996.0137 (1996).

19 Munch, D. *et al.* Identification and in vitro analysis of the GatD/MurT enzyme-complex catalyzing lipid II amidation in Staphylococcus aureus. *PLoS Pathog* **8**, e1002509, doi:10.1371/journal.ppat.1002509 (2012).
20 Hackel, M. A. *et al.* Reproducibility of broth microdilution MICs for the novel siderophore cephalosporin, cefiderocol, determined using iron-depleted cation-adjusted Mueller-Hinton broth. *Diagn Microbiol Infect Dis* **94**, 321-325, doi:10.1016/j.diagmicrobio.2019.03.003 (2019).
21 Ho, S. W. *et al.* Effect of divalent cations on the structure of the antibiotic daptomycin. *European Biophysics Journal* **37**, 421-433, doi:10.1007/s00249-007-0227-2 (2007).
22 Visscher, K. M. *et al.* Supramolecular Organization and Functional Implications of K+ Channel Clusters in Membranes. *Angewandte Chemie International Edition* **56**, 13222-13227, doi:10.1002/anie.201705723 (2017).
23 Etzkorn, M., Böckmann, A., Lange, A. & Baldus, M. Probing Molecular Interfaces Using 2D Magic-Angle-Spinning NMR on Protein Mixtures with Different Uniform Labeling. *Journal of the American Chemical Society* **126**, 14746-14751, doi:10.1021/ja0479181 (2004).
24 van Dam, V. *et al.* Transmembrane transport of peptidoglycan precursors across model and bacterial membranes. *Mol Microbiol* **64**, 1105-1114, doi:10.1111/j.1365-2958.2007.05722.x (2007).
25 Ni, Q. Z. *et al.* High Frequency Dynamic Nuclear Polarization. *Accounts of Chemical Research* **46**, 1933-1941, doi:10.1021/ar300348n (2013).
26 Kaplan, M. *et al.* EGFR Dynamics Change during Activation in Native Membranes as Revealed by NMR. *Cell* **167**, 1241-1251.e1211, doi:10.1016/j.cell.2016.10.038 (2016).
27 Li, S. & Hong, M. Protonation, Tautomerization, and Rotameric Structure of Histidine: A Comprehensive Study by Magic-Angle-Spinning Solid-State NMR. *Journal of the American Chemical Society* **133**, 1534-1544, doi:10.1021/ja108943n (2011).
28 Kodera, N., Yamamoto, D., Ishikawa, R. & Ando, T. Video imaging of walking myosin V by high-speed atomic force microscopy. *Nature* **468**, 72-76, doi:10.1038/nature09450 (2010).
29 Maity, S. *et al.* Caught in the Act: Mechanistic Insight into Supramolecular Polymerization-Driven Self-Replication from Real-Time Visualization. *Journal of the American Chemical Society* **142**, 13709-13717, doi:10.1021/jacs.0c02635 (2020).
30 Melcrová, A. *et al.* Lateral membrane organization as target of an antimicrobial peptidomimetic compound. *Nature Communications* **14**, doi:10.1038/s41467-023-39726-5 (2023).
31 van Beekveld, R. A. M. *et al.* Specific Lipid Studies in Complex Membranes by Solid-State NMR Spectroscopy. *Chemistry – A European Journal* **28**, doi:10.1002/chem.202202472 (2022).
32 Medeiros-Silva, J. *et al.* High-resolution NMR studies of antibiotics in cellular membranes. *Nature Communications* **9**, doi:10.1038/s41467-018-06314-x (2018).
33 Hasper, H. E. *et al.* An Alternative Bactericidal Mechanism of Action for Lantibiotic Peptides That Target Lipid II. *Science* **313**, 1636-1637, doi:10.1126/science.1129818 (2006).
34 Essig, A. *et al.* Copsin, a Novel Peptide-based Fungal Antibiotic Interfering with the Peptidoglycan Synthesis. *Journal of Biological Chemistry* **289**, 34953-34964, doi:10.1074/jbc.M114.599878 (2014).
35 Cudic, P. *et al.* Complexation of peptidoglycan intermediates by the lipoglycodepsipeptide antibiotic ramoplanin: Minimal structural requirements for intermolecular complexation and fibril formation. *Proceedings of the National Academy of Sciences* **99**, 7384-7389, doi:10.1073/pnas.102192099 (2002).
36 Müller, A. *et al.* Daptomycin inhibits cell envelope synthesis by interfering with fluid membrane microdomains. *Proceedings of the National Academy of Sciences* **113**, doi:10.1073/pnas.1611173113 (2016).
37 Yang, H., Chen, K. H. & Nowick, J. S. Elucidation of the Teixobactin Pharmacophore. *ACS Chemical Biology* **11**, 1823-1826, doi:10.1021/acschembio.6b00295 (2016).
38 Horton, R. M., Cai, Z. L., Ho, S. N. & Pease, L. R. Gene splicing by overlap extension: tailor-made genes using the polymerase chain reaction. *Biotechniques* **8**, 528-535 (1990).

39 de Jong, R. N., Daniëls, M. A., Kaptein, R. & Folkers, G. E. Enzyme free cloning for high throughput gene cloning and expression. *J Struct Funct Genomics* **7**, 109-118, doi:10.1007/s10969-006-9014-z (2006).

40 Breukink, E. *et al.* Lipid II is an intrinsic component of the pore induced by nisin in bacterial membranes. *J Biol Chem* **278**, 19898-19903, doi:10.1074/jbc.M301463200 (2003).

41 Danilov, L. L., Druzhinina, T. N., Kalinchuk, N. A., Maltsev, S. D. & Shibaev, V. N. Polyprenyl phosphates: synthesis and structure-activity relationship for a biosynthetic system of Salmonella anatum O-specific polysaccharide. *Chem Phys Lipids* **51**, 191-203, doi:10.1016/0009-3084(89)90006-6 (1989).

42 Cochrane, R. V. K. *et al.* From plant to probe: semi-synthesis of labelled undecaprenol analogues allows rapid access to probes for antibiotic targets. *Chem Commun (Camb)* **56**, 8603-8606, doi:10.1039/d0cc03388j (2020).

43 Rouser, G., Siakotos, A. N. & Fleischer, S. Quantitative analysis of phospholipids by thin-layer chromatography and phosphorus analysis of spots. *Lipids* **1**, 85-86, doi:10.1007/BF02668129 (1966).

44 Hope, M. J., Bally, M. B., Webb, G. & Cullis, P. R. Production of large unilamellar vesicles by a rapid extrusion procedure: characterization of size distribution, trapped volume and ability to maintain a membrane potential. *Biochim Biophys Acta* **812**, 55-65, doi:10.1016/0005-2736(85)90521-8 (1985).

45 Sauvée, C. *et al.* Highly Efficient, Water-Soluble Polarizing Agents for Dynamic Nuclear Polarization at High Frequency. *Angewandte Chemie International Edition* **52**, 10858-10861, doi:10.1002/anie.201304657 (2013).

46 Weingarth, M., Bodenhausen, G. & Tekely, P. Low-power decoupling at high spinning frequencies in high static fields. *J Magn Reson* **199**, 238-241, doi:10.1016/j.jmr.2009.04.015 (2009).

47 Weingarth, M., Tekely, P. & Bodenhausen, G. Efficient heteronuclear decoupling by quenching rotary resonance in solid-state NMR. *Chemical Physics Letters* **466**, 247-251, doi:10.1016/j.cplett.2008.10.041 (2008).

48 Weingarth, M., Demco, D. E., Bodenhausen, G. & Tekely, P. Improved magnetization transfer in solid-state NMR with fast magic angle spinning. *Chemical Physics Letters* **469**, 342-348, doi:10.1016/j.cplett.2008.12.084 (2009).

49 Fung, B. M., Khitrin, A. K. & Ermolaev, K. An improved broadband decoupling sequence for liquid crystals and solids. *J Magn Reson* **142**, 97-101, doi:10.1006/jmre.1999.1896 (2000).

50 Medeiros-Silva, J. *et al.* (1) H-Detected Solid-State NMR Studies of Water-Inaccessible Proteins In Vitro and In Situ. *Angew Chem Int Ed Engl* **55**, 13606-13610, doi:10.1002/anie.201606594 (2016).

51 Doherty, T. & Hong, M. 2D 1H-31P solid-state NMR studies of the dependence of inter-bilayer water dynamics on lipid headgroup structure and membrane peptides. *J Magn Reson* **196**, 39-47, doi:10.1016/j.jmr.2008.10.001 (2009).

52 Gullion, T. Introduction to rotational-echo, double-resonance NMR. *Concepts in Magnetic Resonance* **10**, 277-289, doi:10.1002/(sici)1099-0534(1998)10:5<277::Aid-cmr1>3.0.Co;2-u (1998).

53 Vinod Chandran, C., Madhu, P. K., Kurur, N. D. & Brauniger, T. Swept-frequency two-pulse phase modulation (SWf-TPPM) sequences with linear sweep profile for heteronuclear decoupling in solid-state NMR. *Magn Reson Chem* **46**, 943-947, doi:10.1002/mrc.2285 (2008).

54 Peng, J. W., Thanabal, V. & Wagner, G. 2D heteronuclear NMR measurements of spin-lattice relaxation times in the rotating frame of X nuclei in heteronuclear HX spin systems. *Journal of Magnetic Resonance (1969)* **94**, 82-100, doi:10.1016/0022-2364(91)90296-6 (1991).

55 Jarmoskaite, I., AlSadhan, I., Vaidyanathan, P. P. & Herschlag, D. How to measure and evaluate binding affinities. *Elife* **9**, doi:10.7554/eLife.57264 (2020).